Progress In Electromagnetics Research B, Vol. 29, 311–338, 2011

RADAR CROSS SECTIONS OF SEA AND GROUND CLUTTER ESTIMATED BY TWO SCALE MODEL AND SMALL SLOPE APPROXIMATION IN HF-VHF BANDS

L. Vaitilingom and A. Khenchaf

Laboratory E3I2, ENSTA-Bretagne
2 rue Françis Verny 29806 Brest Cedex 9, France

Abstract—HF-VHF Radars are used in oceanography and sea surveys [1] because they can cover a larger distance than other radars. We can use this kind of radar in sea and ground environments. In these bands, phenomena associated with clutter [2] interfere with radar performance for ship and terrestrial vehicle detection. To improve radar performance, a measure called Radar Cross Section is calculated. We have studied Radar Cross Section in HF-VHF bands with the objective of determining the influence of sea and ground clutter. There are two categories of Radar Cross Section: exact methods [3] and approximate methods [4–8]. We have studied approximate methods because they are faster than exact methods. A common radar configuration is the bistatic configuration where transmitter and receiver are dissociated. The aim of this paper is to study Radar Cross Sections of clutter estimated by approximate models in HF-VHF bands in a bistatic configuration.

1. INTRODUCTION

Mankind has always felt the need to identify objects and their position around itself. To detect and locate objects, man first used his senses. Then, he imagined and built devices such as telescopes and binoculars. Their invention enabled coverage of an increasingly extended range. The discovery of electromagnetic waves led to the invention of radar. A radar transmits an electromagnetic plane wave (composed of an electric field $\vec{E}^i$ and a magnetic field $\vec{H}^i$) which impacts a target. This wave evolves in the $(\vec{h}_i, \vec{v}_i)$ plane in the $\vec{n}_i$ direction with a wave number of

Received 16 February 2011, Accepted 30 March 2011, Scheduled 15 April 2011
Corresponding author: Laurent Vaitilingom (laurent.vaitilingom@ensta-bretagne.fr).

k rad/m. The target radiates electromagnetic waves in all directions. A number of these scattered electromagnetic waves go to the receiver in the $\vec{n}_s$ direction in the $(\vec{h}_s, \vec{v}_s)$ plane. These scattered waves give us information as to the nature and the position of the target.

The transmitting base $(\vec{h}_i, \vec{v}_i, \vec{n}_i)$ and the scattered base $(\vec{h}_s, \vec{v}_s, \vec{n}_s)$ are linked to the global base $(\vec{x}, \vec{y}, \vec{z})$ by:

$$\begin{cases} \vec{h}_i = -\sin\phi_i\vec{x} + \cos\phi_i\vec{y} \\ \vec{v}_i = -\cos\theta_i\cos\phi_i\vec{x} - \cos\theta_i\sin\phi_i\vec{y} - \sin\theta_i\vec{z} \\ \vec{n}_i = \sin\theta_i\cos\phi_i\vec{x} + \sin\theta_i\sin\phi_i\vec{y} - \cos\theta_i\vec{z} \end{cases} \quad (1)$$

$$\begin{cases} \vec{h}_s = -\sin\phi_s\vec{x} + \cos\phi_s\vec{y} \\ \vec{v}_s = \cos\theta_s\cos\phi_s\vec{x} + \cos\theta_s\sin\phi_s\vec{y} - \sin\theta_s\vec{z} \\ \vec{n}_s = \sin\theta_s\cos\phi_s\vec{x} + \sin\theta_s\sin\phi_s\vec{y} + \cos\theta_s\vec{z} \end{cases} \quad (2)$$

$\vec{z}$ is the normal unitary vector to the surface at impact point and $(\vec{x}, \vec{y})$ the tangent plane to the surface. $(\vec{x}, \vec{y}, \vec{z})$ is the global base. A bistatic angle ϕ_0 is also defined by:

$$\cos(2\phi_0) = \cos\theta_i\cos\theta_s - \sin\theta_i\sin\theta_s\cos(\phi_s - \phi_i) \quad (3)$$

The expression of incident electrical wave field is:

$$\vec{E}^i = E_0 \cdot e^{-jk\vec{n}_i\cdot\vec{r}} \quad (4)$$

Stratton-Chu wrote an expression of total electrical field which takes into account the transmitting wave [8, 9]:

$$\vec{E}^s = -jk\frac{e^{-jkR_0}}{4\pi R_0}\cdot\vec{n}_s \times \int_S \left[\vec{n}\times\vec{E}^i - \eta_s\cdot\vec{n}_s\times\left(\vec{n}\times\vec{H}^i\right)\right]\cdot e^{jk\vec{r}\vec{n}_s}ds \quad (5)$$

To help radars to identify and locate a target, Polarimetric Radar Cross Section is calculated:

$$\sigma_{pq} = 4\pi R_0^2\frac{\left\langle E^s_{pq}E^{s*}_{pq}\right\rangle}{E^i_q E^{i*}_q} \quad (6)$$

where E^i_q is the q polarization component of E^i. The incident electromagnetic wave can be written:

$$E^i_q = \vec{q}\cdot E_0\cdot e^{-jk\vec{n}_i\cdot\vec{r}} \quad (7)$$

E^s_{pq} stands for the scattered field component p when the transmitting polarisation is q. $\langle\rangle$ is the mean operator. a^* is the conjugate of a. R_0 is the distance between the target and the receiver.

In oceanography and coastal surveys [1], HF-VHF radars are used (to detect boats far from the coast, plane low-flying or to study ocean currents) because they cover a larger distance than other radars such as X-band radars (even if there are more simulations and

experiments in bands higher than the VHF band [10, 11]). Since the creation of Exclusive Economic Zones (EEZ) in 1982, interest in HF-VHF radars has increased and countries are now equipped by HF-VHF radars: OSMAR in China [12], WERA in Germany [13, 14], NOSTRADAMUS in France [15], ... In HF-VHF bands, there are two problems: the height of the antenna which can be huge and clutter which, if its level is too high, can stop us from detecting a target. Solutions such as MLA technology [16] or CODAR [17] enable the problem of antenna dimension to be solved. Environmental and ionospheric clutter interferes with radar performance [2]. Ionospheric clutter in HF-VHF bands has recently been dealt with by scientists such as Jangal [18], Vallières [19] or Wan [12]. Phenomena linked to environmental clutter (such as Bragg's wave) also affect radar performance of detection. In 1955, Crombie highlighted the presence of Bragg's waves. Interested in observations made by Crombie, Barrick [6, 20–23] developed a monostatic (transmitter co-located with receiver) sea RCS model related to Doppler frequency. At the same time, using a different approach, Walsh et al. obtained the same results as Barrick. Gill extended this model to bistatic configuration [7, 24–27]. Recently, the Walsh and Gill model was proved to be efficient in an HF radar image simulator [28]. In 2008, Gill created a model combining sea clutter and noise [29]. RCS estimated by Gill's model also depends on bistatic angle ϕ_0, however this is only in vertical polarization. There are few models that can be compared for ground surface [4]. To understand the parameters that govern the intensity of clutter in a radio link, we estimate the Radar Cross Section of sea or ground surfaces in the HF-VHF band. Radar Cross Section estimators can be divided into two categories: exact methods [3, 30] and approximate methods [8, 9]. There are already comparisons between models [11] but these comparisons are in transmitting frequency bands higher than VHF bands.

In this article, we will further comparisons made in 2010 [31] and add comparisons of ground surface to obtain a complete description of a natural surface (sea or ground) electromagnetic signature. We studied RCS estimated by approximate methods because they are faster and need less memory space than exact methods. To use approximate methods, we need to characterize a surface geometrically and physically. To characterize a surface geometrically, we model height spectrum and/or slope probability. To characterize a surface physically, we examine electrical permittivity and magnetic permeability. Firstly, we will detail the RCS models we used. Secondly, we will characterize the surface. Thirdly, we will observe the results. Finally, we will conclude.

2. RADAR CROSS SECTION MODELS

The Radar Cross Section of a target gives us information as to the nature and the position of the target. Radar Cross Section models are either exact methods or approximate methods. In this paper, we studied approximate methods because they are faster than exact methods. We will firstly examine Gill's model. Secondly, we will concentrate on the Kirchhoff Approximation. Thirdly, we will look at the Small Perturbation Model. Fourthly, we will study the Two Scale Model. Fifthly, we will consider Small Slope Approximation. Finally, we will give conditions of use of these models.

2.1. Gill's Model

Gill [7, 17, 26, 32, 33] created a RCS model to study sea surface. His model is based on Barrick's work [6, 17, 20–23, 32, 33]. This method takes Doppler frequency into account and enables Bragg frequencies to be calculated. Gill's hypothesis is that the single reflection, the double reflection to the transmitter, to the receiver and to the patch contribute to the calculation of the RCS.

The RCS estimated by Gill [28, 31] is expressed by:

$$\sigma^{Gill} = \sigma_{11} + \sigma_{2T} + \sigma_{2R} + \sigma_{2P} \tag{8}$$

where σ_{11}, σ_{2T}, σ_{2R}, σ_{2P} respectively stand for the contributions of the single reflection, the double reflection to the transmitter, the double reflection to the receiver and the double reflection to the patch (Figure 2).

This model is valid for grazing angles, calculated in a vertical polarization and applied to a sea surface. The assumption made by Barrick that the surface is a perfect conductor restricts the use of Gill's model to sea surface. The following models can be applied to both a sea surface and a ground surface.

2.2. The Kirchhoff Approximation

Historically, the first approximate model was the Kirchhoff Approximation [34, 35]. To simplify the quantities $\vec{n} \times \vec{E}$ and $\vec{n} \times \vec{H}$ in the Equation (5), the Kirchhoff Approximation considers that a surface around any point is equivalent to a tangent plane at this point. This hypothesis is valid if the mean curvature radius of the surface is larger than the transmitting wavelength.

We create a local base $(\vec{t}, \vec{d}, \vec{n})$ such that:

$$\begin{cases} \vec{t} = \|\vec{n}_i \times \vec{n}\|^{-1} (\vec{n}_i \times \vec{n}) \\ \vec{d} = \vec{n}_i \times \vec{t} \\ \vec{n} = \vec{z} \end{cases} \tag{9}$$

This base permits us to express scattered electric field in terms of Fresnel coefficients:

$$\vec{E}^s = -jk \frac{e^{-jkR_0}}{4\pi R_0} \vec{n}_s \times \int \vec{P} \cdot e^{jk\vec{r}(\vec{n}_s - \vec{n}_i)} dS \tag{10}$$

where

$$\begin{aligned} \vec{P} \;=\; & E_0 \Big[(1 + R_h)(\vec{q} \cdot \vec{t})(\vec{n} \times \vec{t}) - (1 - R_v)(\vec{n} \cdot \vec{n}_i)(\vec{q} \cdot \vec{d}) \cdot \vec{t} \\ & -(1 - R_h)(\vec{q} \cdot \vec{t})(\vec{n} \cdot \vec{n}_i) \cdot \vec{t} + (1 + R_v)(\vec{n} \times \vec{t})(\vec{q} \cdot \vec{d}) \Big] \end{aligned}$$

R_h and R_v are reflection coefficients in respectively horizontal and vertical polarisation.

If we consider that the phase is stationary:

$$\vec{E}^s = -jk \frac{e^{-jkR_0}}{4\pi R_0} \vec{n}_s \times \vec{P} \cdot \int e^{j\vec{Q}} dS \tag{11}$$

Q denotes the phase:

$$\vec{Q} = k\vec{r}(\vec{n}_s - \vec{n}_i) = q_x \vec{x} + q_y \vec{y} + q_z \vec{z} \tag{12}$$

Its coordinates are:

$$\begin{cases} q_x & = k(\sin\theta_s \cos\phi_s - \sin\theta_i \cos\phi_i) \\ q_y & = k(\sin\theta_s \sin\phi_s - \sin\theta_i \sin\phi_i) \\ q_z & = k(\cos\theta_s + \cos\theta_i) \\ \| \vec{Q} \|^2 & = q_x^2 + q_y^2 + q_z^2 \\ & = 2k^2 \times [1 + \cos\theta_s \cos\theta_i - \sin\theta_s \sin\theta_i \cos(\phi_s - \phi_i)] \end{cases}$$

$\| \vec{Q} \|^2$ is the norm of $\vec{Q}$. Stationary condition is valid if:

$$\begin{cases} \frac{\partial Q}{\partial x} = 0 = q_x + q_z \cdot Z_x \\ \frac{\partial Q}{\partial y} = 0 = q_y + q_z \cdot Z_y \end{cases} \tag{13}$$

where Z_x and Z_y stand for surface slope in respect to x and y directions respectively.

The local base can be expressed in relation to the phase coordinates:

$$\begin{cases} \vec{n} = \frac{k|q_z|(\vec{n}_i - \vec{n}_s)}{q^2 q_z} \\ \vec{t} = \frac{|q_z|(\vec{n}_i \times \vec{n})}{q_z D} \\ \vec{d} = \frac{|q_z|((\vec{n}_i \cdot \vec{n}_s) \cdot \vec{n}_i - \vec{n}_s)}{q_z D} \end{cases} \tag{14}$$

$$D = \sqrt{(\vec{n}_i \cdot \vec{v}_s)^2 + (\vec{n}_i \cdot \vec{h}_s)^2}$$

Polarimetric Radar Cross Section estimated by Kirchhoff Approximation becomes:

$$\sigma_{pq} = \frac{\pi k^2 \parallel \vec{Q} \parallel^2}{q_z^4} \cdot |U_{pq}|^2 \cdot Prob\left(-q_x/q_z, -q_y/q_z\right) \tag{15}$$

Where U_{pq} are Kirchhoff polarization parameters depending on polarization, incident wavenumber, relative electrical permittivity ϵ_r, relative magnetic permeability μ_r, and incident, azimuthal incident, scattered and azimuthal scattered angles and is given in [8]:

$$\begin{aligned}
U_{hh} &= \frac{q\,|q_z|\left\{R_{\parallel}\,(\vec{h}_s.\vec{n}_i)(\vec{h}_i.\vec{n}_s) + R_{\perp}(\vec{v}_s.\vec{n}_i)(\vec{v}_i.\vec{n}_s)\right\}}{[(\vec{n}_i.\vec{h}_s)^2 + (\vec{n}_i.\vec{v}_s)^2]kq_z} \\
U_{hv} &= \frac{q\,|q_z|\left\{R_{\parallel}\,(\vec{h}_s.\vec{n}_i)(\vec{v}_i.\vec{n}_s) - R_{\perp}(\vec{v}_s.\vec{n}_i)(\vec{h}_i.\vec{n}_s)\right\}}{[(\vec{n}_i.\vec{v}_s)^2 + (\vec{n}_i.\vec{h}_s)^2]kq_z} \\
U_{vh} &= \frac{q\,|q_z|\left\{R_{\parallel}\,(\vec{v}_s.\vec{n}_i)(\vec{h}_i.\vec{n}_s) - R_{\perp}(\vec{h}_s.\vec{n}_i)(\vec{v}_i.\vec{n}_s)\right\}}{[(\vec{n}_i.\vec{h}_s)^2 + (\vec{n}_i.\vec{v}_s)^2]kq_z} \\
U_{vv} &= \frac{q\,|q_z|\left\{R_{\parallel}\,(\vec{v}_s.\vec{n}_i)(\vec{v}_i.\vec{n}_s) + R_{\perp}(\vec{h}_s.\vec{n}_i)(\vec{h}_i.\vec{n}_s)\right\}}{[(\vec{n}_i.\vec{v}_s)^2 + (\vec{n}_i.\vec{h}_s)^2]kq_z}
\end{aligned} \tag{16}$$

With:

$$\begin{aligned}
R_{||} &= \frac{\epsilon_r \cos(\theta_l) - \sqrt{\mu_r\epsilon_r - \sin^2(\theta_l)}}{\epsilon_r \cos(\theta_l) + \sqrt{\mu_r\epsilon_r - \sin^2(\theta_l)}} \\
R_{\perp} &= \frac{\mu_r \cos(\theta_l) - \sqrt{\mu_r\epsilon_r - \sin^2(\theta_l)}}{\mu_r \cos(\theta_l) + \sqrt{\mu_r\epsilon_r - \sin^2(\theta_l)}}
\end{aligned}$$

And:

$$\cos(\theta_l) = \frac{\sqrt{1 - \sin(\theta_i)\sin(\theta_s)\cos(\varphi_i - \varphi_s) + \cos(\theta_i)\cos(\theta_s)}}{\sqrt{2}}$$

$Prob(Z_x, Z_y)$ is the joint probability of surface slope in x direction Z_x and y direction Z_y.

This model is valid for a surface with a mean curvature radius greater than the incidence wavelength and is applied to a surface with large roughness. For a surface with small roughness, we used the Small Perturbation Model.

2.3. The Small Perturbation Method

We applied the Small Perturbation Method [4, 31, 34–36] to determine the RCS of a surface with small roughness. The hypothesis is that the

total field in a zone is the sum of plane waves with unknown amplitudes. In our study, there are 3 kinds of electric fields: incident fields, specular fields and non-specular fields. In the introduction, we said that the incident electromagnetic wave is a plane wave. So the specular wave is also a plane wave. Consequently, non-specular waves are plane waves with unknown amplitudes:

$$\vec{E}^s_{pq} = \frac{1}{2\pi}\int_{-\infty}^{\infty}\int_{-\infty}^{\infty}\vec{A}_{pq}(k_x,k_y)e^{j(k_x x+k_y y-k_z z)}dk_x dk_y \tag{17}$$

where

$$\begin{cases} k_x = k(-\sin\theta_s\cos\phi_s + \sin\theta_i\cos\phi_i) \\ k_y = k(-\sin\theta_s\sin\phi_s + \sin\theta_i\sin\phi_i) \\ k_z = k(\cos\theta_s + \cos\theta_i) \end{cases}$$

If the surface we study is with small roughness, we can substitute the exponential term by its Taylor series:

$$e^{-jk_z z(x,y)} = 1 - jk_z z(x,y) - \frac{(k_z z(x,y))^2}{2} + \ldots$$

The scattered electric field becomes:

$$\vec{E}^s_{pq} = \frac{1}{2\pi}\int_{-\infty}^{\infty}\int_{-\infty}^{\infty}\vec{A}_{pq}\times(1-jk_z z(x,y)+\ldots)\,e^{j(k_x x+k_y y)}dk_x dk_y \tag{18}$$

The RCS estimated by the Small Perturbation Method is:

$$\sigma_{pq} = 8k^3\left|\cos\theta_i\cos\theta_s\alpha_{pq}\right|^2 S(k_x,k_y) \tag{19}$$

where k is the incident wavenumber. θ_i is incident angle and θ_s is scattered angle. α_{pq} is the polarization parameters depending on polarization, incident wavenumber, electrical permittivity, magnetic permeability, and incident, azimuthal incident, scattered and azimuthal scattered angles and is given in [8]:

$$\begin{aligned}
\alpha_{h_s h_i} =& \frac{[k'_z k'_i.\cos(\phi_s-\phi_i) - \mu_r\sin(\theta_i)\sin(\theta_s)]\,(\mu_r-1)}{(\mu_r\cos(\theta_s)+k'_z)\,[\mu_r\cos(\theta_i)+k'_i]} \\
&- \frac{\mu_r^2(\epsilon_r-1)\cos(\phi_s-\phi_i)}{(\mu_r\cos(\theta_s)+k'_z)\,[\mu_r\cos(\theta_i)+k'_i]} \\
\alpha_{h_s v_i} =& \frac{[(\epsilon_r-1)\mu_r k'_i - \epsilon_r(\mu_r-1)k'_z]\sin(\phi_s-\phi_i)}{(k'_z+\mu_r\cos(\theta_s))\,[\epsilon_r\cos(\theta_i)+k'_i]} \\
\alpha_{v_s h_i} =& \frac{[(\mu_r-1)\epsilon_r k'_i - \mu_r(\epsilon_r-1)k'_z]\sin(\phi_s-\phi_i)}{(k'_z+\epsilon_r\cos(\theta_s))\,[\mu_r\cos(\theta_i)+k'_i]} \\
\alpha_{v_s v_i} =& \frac{[k'_z k'_i\cos(\phi_s-\phi_i) - \epsilon_r\sin(\theta_i)\sin(\theta_s)]\,(\epsilon_r-1)}{(\epsilon_r\cos(\theta_s)+k'_z)\,[\epsilon_r\cos(\theta_i)+k'_i]} \\
&- \frac{\epsilon_r^2(\mu_r-1)\cos(\phi_s-\phi_i)}{(\epsilon_r\cos(\theta_s)+k'_z)\,[\epsilon_r\cos(\theta_i)+k'_i]}
\end{aligned} \tag{20}$$

With $k'_i = \sqrt{\epsilon_r \mu_r - \sin^2(\theta_i)}$ and $k'_z = \sqrt{\epsilon_r \mu_r - \sin^2(\theta_s)}$.

S is the surface height spectrum, k_x and k_y is the spatial wavenumber in respectively x and y directions.

The Small Perturbation Method is only applied to a surface with small roughness.

2.4. The Two Scale Method

The two previous models can only be applied to a single roughness scale. A natural surface has two (or more) roughness scales. To take into account the double roughness scales of clutter, unified methods which are combinations of the two previous models were used. One of these methods is the Two Scale Method [5, 8, 9, 31, 37]. By applying Two Scale Model, Radar Cross Section is calculated by averaging Radar Cross Section over surface slope. Radar Cross Section for a surface slope is obtained by projections on global basis of Radar Cross Section estimated in local basis. Radar Cross Section estimated in local basis is estimated by Small Perturbation Method. A global

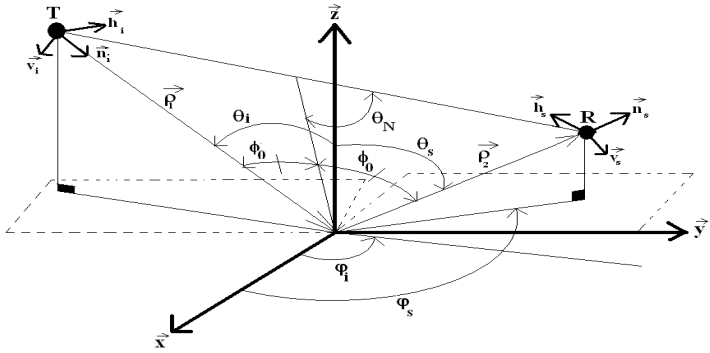

Figure 1. Radar configuration.

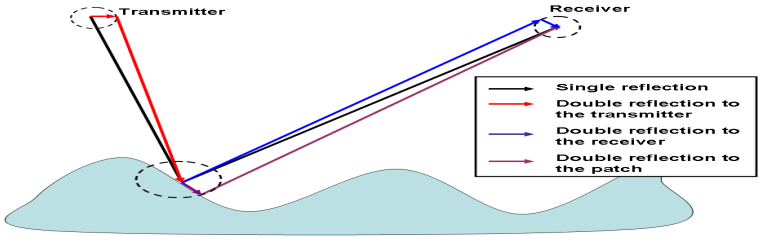

Figure 2. Gill's model.

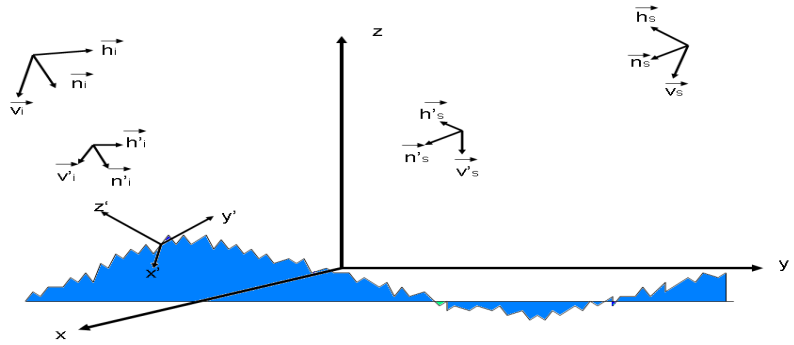

Figure 3. TSM bases.

base $(\vec{x}, \vec{y}, \vec{z})$ is created which is independent from the surface. The transmitting global base $(\vec{h}_i, \vec{v}_i, \vec{n}_i)$ and receiving global base $(\vec{h}_s, \vec{v}_s, \vec{n}_s)$ are created in the same way in Figure 1. The local base $(\vec{x}', \vec{y}', \vec{z}')$, local transmitting base $(\vec{h}'_i, \vec{v}'_i, \vec{n}'_i)$ and local receiving base $(\vec{h}'_s, \vec{v}'_s, \vec{n}'_s)$ are created. The local base $(\vec{x}', \vec{y}', \vec{z}')$ is linked to the surface. $\vec{z}'$ is the normal to the surface. $(\vec{x}', \vec{y}')$ is the tangent plane to the surface. The local bases are linked the same way than the global bases (Figure 3).

Relations between local and global basis are given by Khenchaf in [8, 9].

The transmitting and scattered fields are written:

$$\begin{aligned} \vec{E}^i_q &= E^i_{h'_i}\vec{h}'_i + E^i_{v'_i}\vec{v}'_i = \left[(q\cdot\vec{h}'_i)\vec{h}'_i + (q\cdot\vec{v}'_i)\vec{v}'_i\right] E_0 \\ \vec{E}^s_{pq} &= E^s_{h'_s}\cdot\vec{h}'_s + E^s_{v'_s}\cdot\vec{v}'_s \end{aligned} \tag{21}$$

The received field and transmitting field are linked by the Sinclair matrix $[M]$:

$$\vec{E}^s = [M]\vec{E}^i \tag{22}$$

where $[M]$ is expressed by:

$$[M] = \begin{bmatrix} \vec{v}'_s\cdot\vec{v}_s & \vec{h}'_s\cdot\vec{v}_s \\ \vec{v}'_s\cdot\vec{h}_s & \vec{h}'_s\cdot\vec{h}_s \end{bmatrix} \begin{bmatrix} M_{v'_s v'_i} & M_{v'_s h'_i} \\ M_{h'_s v'_i} & M_{h'_s h'_i} \end{bmatrix} \begin{bmatrix} \vec{v}'_i\cdot\vec{v}_i & \vec{h}'_i\cdot\vec{v}_i \\ \vec{v}'_i\cdot\vec{h}_i & \vec{h}'_i\cdot\vec{h}_i \end{bmatrix} \tag{23}$$

The scattered field becomes:

$$E^s_{pq} = (\vec{v}'_i\cdot q)\left[(p\cdot\vec{v}'_i)M_{v'_s v'_i} + (p\cdot\vec{h}'_i)M_{v'_s h'_i}\right] \tag{24}$$

We deduce:

$$\begin{aligned}\sigma_{pq}^{s} &= \frac{4\pi R^2}{A}.\frac{\left\langle \left|E_{pq}^{s}\right|^2 \right\rangle}{\left|E_{q}^{i}\right|^2} = \langle G\left(Z_x, Z_y\right)\rangle \\ &= \big\langle (p.\vec{v}_s')^2\,(q.\vec{v}')^2\sigma_{v_s'v'} + (p.\vec{v}_s')^2(q.\vec{h}')^2\sigma_{v_s'h'} \\ &\quad +(p.\vec{h}_s')^2(q.\vec{v}')^2\sigma_{h_s'v'} + (p.\vec{h}_s')^2(q.\vec{h}')^2\sigma_{h_s'h'} \\ &\quad +(p.\vec{h}_s')^2(q.\vec{v}')(q.\vec{h}')\sigma_{h_s'h'h_s'v'} \\ &\quad +(p.\vec{v}_s')(p.\vec{h}_s')(q.\vec{h}')^2\sigma_{h_s'h'v_s'h'} \\ &\quad +(p.\vec{v}_s')(p.h_s')(q.\vec{v}')(q.\vec{h}')\sigma_{v_s'v'h_s'h'} \\ &\quad +(p.\vec{v}_s')(p.h_s')(q.\vec{h}')(q.\vec{v}')\sigma_{h_s'v'v_s'h'} \\ &\quad +(p.\vec{v}_s')(p.\vec{h}_s')(q.\vec{v}')^2\sigma_{h_s'v'v_s'v'} \\ &\quad +(p.\vec{v}_s')^2(q.\vec{h}')(q.\vec{v}')\;\sigma_{v_s'v'v_s'h'}\big\rangle \end{aligned} \tag{25}$$

In local basis, Radar Cross Section is estimated by Small Perturbation Model:

$$\begin{aligned}\sigma_{p'q'r's'} &= 16k^3\cos^2\theta_i'\cos^2\theta_s'\mathrm{Re}(\alpha_{p'q'}\alpha_{r's'}^{*})S^S(k_x + k\sin\theta_i', k_y) \\ \sigma_{p'q'} &= 8k^3\cos^2\theta_i'\cos^2\theta_s'\left|\alpha_{p'q'}\right|^2 S^S(k_x + k\sin\theta_i', k_y)\end{aligned} \tag{26}$$

Where

$$S^S(k_x, k_y) = \begin{cases} S(k_x, k_y), & \sqrt{k_x^2 + k_y^2} > k_d \\ 0, & \sqrt{k_x^2 + k_y^2} < k_d \end{cases}$$

We choose $k_d = k/3$ where k is incident wave number and $\alpha_{p'q'}$ has the same expression that polarization parameters of SPM in Equation (21).

The average is obtained with surface slope probability by:

$$\langle G\rangle = \iint G(Z_x, Z_y)\cdot Prob(Z_x, Z_y)\cdot I dZ_x dZ_y \tag{27}$$

with:

$$I = \begin{cases} 1 \begin{cases} si\,\vec{n}_i\cdot\vec{n} < 0 \\ et\,\vec{n}_i\cdot\vec{n} > 0 \end{cases} \\ 0 \end{cases}$$

This model takes into account the double roughness scale but the parameter (k_d) which distinguishes a surface with large roughness from a surface with small roughness is arbitrary. To conciliate the two scales of surface in a way smoother than Two Scale Model, Small Slope Approximation was created.

2.5. The Small Slope Approximation

The Small Slope Approximation is, like Two Scale Model, an unified model. It means that this model conciliates the Kirchhoff Approximation and the Small Perturbation Model to extend application domains to surfaces with several roughness scales. Radar Cross Section estimated by SSA [38] to the first order is written:

$$\sigma_{pq} = 8\left|\frac{q_k q_0}{q_k + q_0}\alpha_{pq}\right|^2 \cdot \int_0^\infty \left\{e^{-\kappa^2(C_0 - C(r))} - e^{-\kappa^2 C_0}\right\} J_0(Mr) r dr \tag{28}$$

$$M = k\sqrt{(\sin\theta_s \cos\phi_s - \sin\theta_i \cos\phi_i)^2 + (\sin\theta_s \sin\phi_s - \sin\theta_i \sin\phi_i)^2}$$

where $\kappa = q_0 + q_k$, $q_k = k\cos\theta_s$ and $q_0 = k\cos\theta_i$. $C(r)$ stands for auto correlation function. To calculate the auto correlation function, we use the inverse Fourier transform of the sea (or ground) height spectra. C_0 is the first value of the surface auto correlation function. α_{pq} is the same polarization coefficients used in Small Perturbation Model [38]. J_0 is the Bessel coefficient of order zero.

2.6. Conditions of Use of Models

To model Radar Cross Section of clutter approximate models are preferred when we want faster models which need less memory space: the Kirchhoff Approximation, the Small Perturbation Model, the Two Scale Model, the Small Slope Approximation, the Weighted Curvature Approximation, ... Gill created a Radar Cross Section Model dedicated to sea surfaces and working in HF-VHF bands. He established the hypothesis that the surface is a perfect conductor which implicates that electrical permittivity has a high value. Except for Gill's model, all Radar Cross Section models need knowledge of electrical permittivity to be implemented. The estimation of Radar Cross Section by Kirchhoff Approximation requires the computation of Slope probability. This model is valid for surface with large roughness. The estimation of Radar Cross Section by the Small Perturbation Model requires the computation of the Surface Height Spectrum. This model is valid for a surface with small roughness. A natural surface has (at least) two roughness scales. Unified models (the Two Scale Model, the Small Slope Approximation, the Weighted Curvature Approximation, ...) are built according to this principle. Therefore, to estimate a Radar Cross Section using these models, we need to know the slope probability and height spectrum.

3. CLUTTER CHARACTERIZATION

To use Radar Cross Section models, we need to characterize clutter geometrically and physically. To characterize a surface geometrically, we examined slope probability and/or height spectrum. To characterize clutter physically we examined the magnetic permeability and electrical permittivity. We assumed that the surfaces we meet were not magnetic. So their magnetic permeability is equal to vacuum magnetic permeability.

3.1. Slope Probability

Sea slope probability and ground slope probability do not depend on the same parameters. Sea slope probability depends on wind speed $U_{12.5}$ and the difference between wind direction and observation direction (Figure 4). In the following sentences, we will define the difference as wind direction. We use Cox and Munk probability [39–42] to model sea slope probability in HF-VHF bands because this model accommodates an increase in slope due to wind speed and asymmetry of slope in accordance with wind direction.

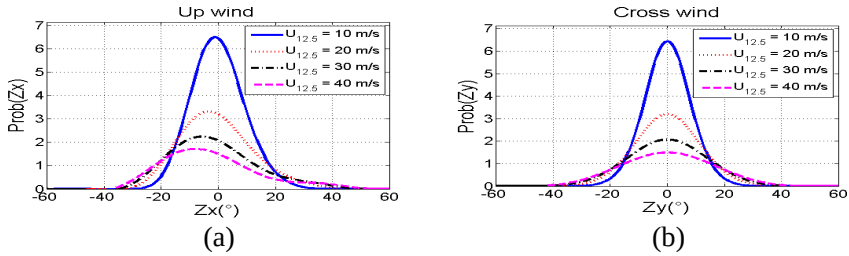

Figure 4. Sea slope probability. (a) Up wind. (b) Cross wind.

Ground slope probability does not depend on wind (Figure 5).

We employed Gauss distribution to model ground slope probability. According to this model, ground slope probability depends on height standard deviation in x direction, σ_u and y direction σ_c.

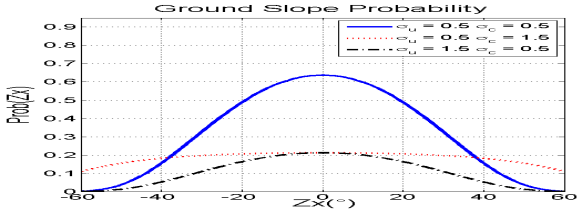

Figure 5. Ground slope probability.

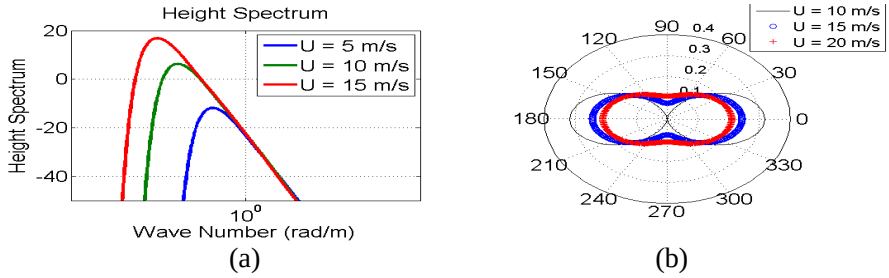

Figure 6. Sea spectrum. (a) Isotropic spectrum. (b) Spread function.

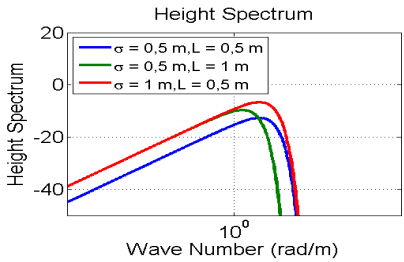

Figure 7. Ground spectrum.

3.2. Height Spectrum

Height spectrum is the Fourier transform of the autocorrelation of the surface. Sea height spectrum depends on wind speed U and wind direction (Figure 6). Sea height spectrum $S(K, \phi)$ is written as the product of isotropic part $S(K)$ by spread function $f(K, \phi)$ where K is the spatial wavenumber and ϕ is the difference between observation direction and wind direction.

To model sea height spectrum, we used the Elfouhaily spectrum [43]. According to this model, gravity waves grow when wind speed increases but capillarity waves do not change. This model shows us that the more the difference between wind direction and observation direction increases, the more the height spectrum decreases. This model depends also on fetch. Elfouhaily calculates the inverse of wave age Ω knowing the fetch using the relation [43]:

$$\Omega = 0.84 \left[\tanh \left(\frac{X}{2.2 \times 10^4} \right)^{0.4} \right]^{-0.75}$$

Ground height spectrum depends on height standard deviation and correlation length (Figure 7).

To model ground height spectrum, we employed the Gaussian spectrum. According to this model, an increase in height standard deviation engenders an increase in height spectrum. An augmentation in correlation length causes a shift in height spectrum to a low spatial wavenumber.

3.3. Electrical Permittivity

The electrical permittivity is the physical property which describes the response of a given medium to an applied electrical field.

To model sea electrical permittivity, we employed the Debye model [5, 8, 38, 44].

This model takes into account the dependence of electrical permittivity on sea temperature (noted T in Figure 8), salinity (noted S in Figure 8) and incident wave frequency.

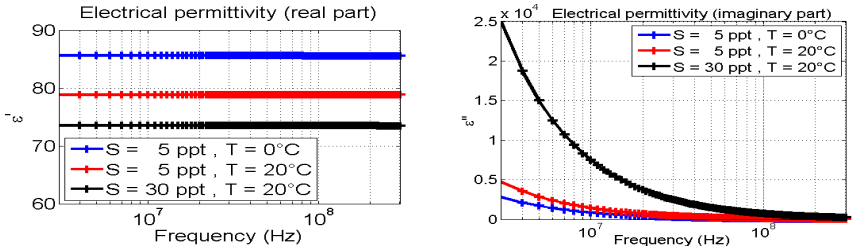

Figure 8. Sea electrical permittivity estimated by Debye model. (a) Real sea electrical permittivity. (b) Imaginary sea electrical permittivity.

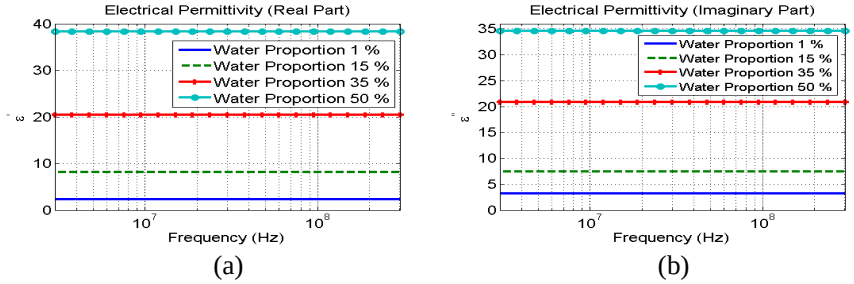

Figure 9. Ground permittivity in relation to transmitting frequency estimated by Topp model. (a) Real ground electrical permittivity. (b) Imaginary ground electrical permittivity.

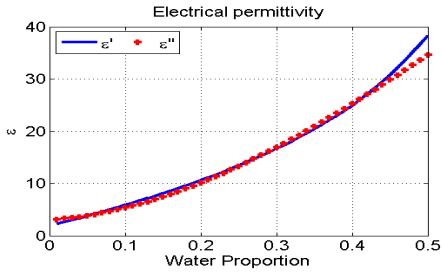

Figure 10. Ground permittivity in relation to water proportion estimated by Topp model.

To model ground permittivity, we used the Topp model [4] which is valid between 20 MHz and 1 GHz.

This model shows us the dependence of ground electrical permittivity on the proportion of water in the surface. The higher the water proportion the higher the ground electrical permittivity (Figures 9 and 10).

4. RESULTS

In this part of our study, we will examine the RCS estimated by approximate models in HF-VHF band for a sea and a ground surface in function of different parameters. We will see the evolution of the RCS in relation to angles and transmitting frequency. For a sea surface full developed (a fetch of 10^{10} m), we will observe the effects of wind (speed and direction) and Doppler frequency. For a ground surface, we will observe the effects of correlation length, height standard deviation and water proportion.

4.1. Sea Surface

The following simulations of RCS of sea surface was made for a temperature of 20° and a salinity of 35 ppt. The evolution of sea clutter monostatic RCS in relation to Doppler frequency is represented in Figures 11 and 12 for an incident angle of 85°, a transmitting frequency of 25 MHz, a windspeed of 5 m/s and a wind direction of 0°. Each component σ_{11}, σ_{2T}, σ_{2P} and σ_{2R} of the RCS estimated by Gill are represented in Figure 11.

The total RCS, which is the sum of all components σ_{11}, σ_{2T}, σ_{2P} and σ_{2R} estimated by Gill, is represented in Figure 12.

The RCS estimated by Gill is also a result of the bistatic angle, transmitting frequency, wind speed and direction. To evaluate the RCS estimated by (SPM,TSM and Gill's model) in relation to these

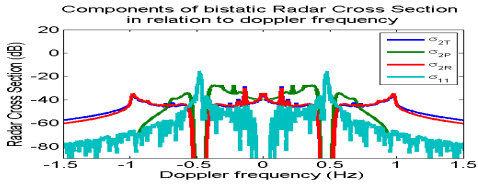

Figure 11. Evolution of components of the RCS in relation to the Doppler frequency.

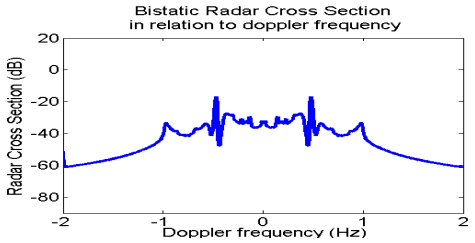

Figure 12. Evolution of the RCS in relation to the Doppler frequency.

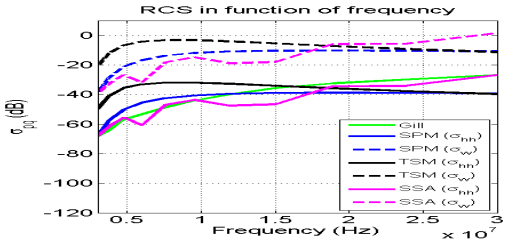

Figure 13. Evolution of the RCS in relation to the transmitting frequency.

parameters, we integrated the RCS estimated by Gill over Doppler frequency.

The Figure 13 shows the evolution of RCS in a vertical and horizontal polarization in relation to transmitting frequency estimated by Gill, SPM, TSM and SSA in a monostatic configuration with $\theta_s = \theta_i = 75°$ ($\phi_0 = 0°$), wind speed $U_{10} = 5\,\mathrm{m/s}$ and wind direction of 0°.

The Figure 14 shows the evolution of the RCS in a vertical polarization resulting from the bistatic angle estimated by Gill, SPM and TSM for a transmitting frequency of 25 MHz, with $\theta_s = \theta_i = 85°$, a wind speed of 5 m/s and a wind direction of 0°.

The Figure 15 shows the evolution of the RCS in relation to wind speed in a vertical polarization in a bistatic case for a transmitting

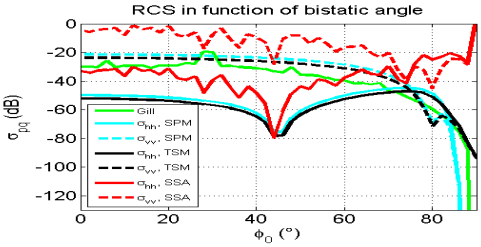

Figure 14. Evolution of the RCS in relation to the bistatic angle.

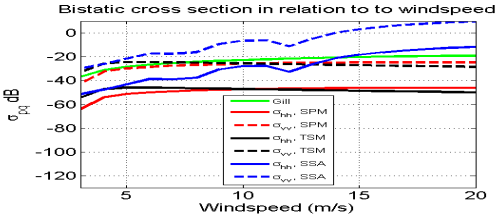

Figure 15. Evolution of the RCS in relation to the wind speed.

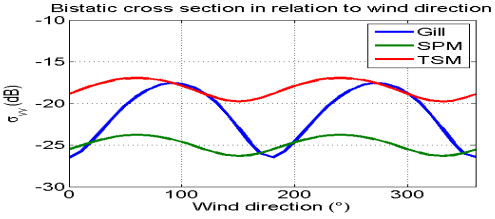

Figure 16. Evolution of the RCS in relation to the wind direction.

frequency of 25 MHz, with $\theta_s = \theta_i = 75°$, $\phi_s = 60°$, $\phi_i = 0°$ and a wind direction of 0°.

The Figure 16 shows the evolution of the RCS in relation to wind direction in a vertical polarization for a bistatic ($\phi_0 = 60°$, $\theta_i = \theta_s = 85°$, $\phi_s \approx 60°$) case for a transmitting frequency of 25 MHz and a wind speed of 5 m/s.

Gill's model is an extension of monostatic Barrick's model to a bistatic model. Barrick's model depends on Doppler frequency but Barrick also made some modelisations of Radar Cross Section in relation to incident angle (Figure 17). In Figure 17, incident angle from the surface is designed by grazing angle. It is interesting to compare this simulation made by Barrick it can be used as a reference.

For an incident frequency less than 7 MHz, to augment the RCS in

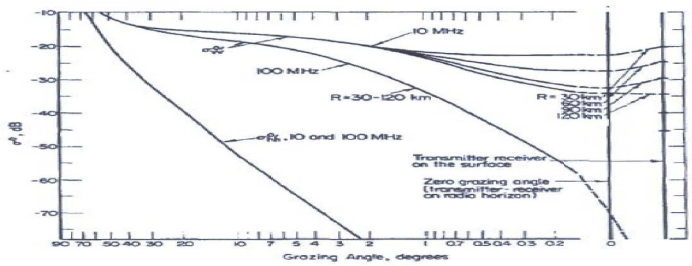

Figure 17. Barrick's RCS [22].

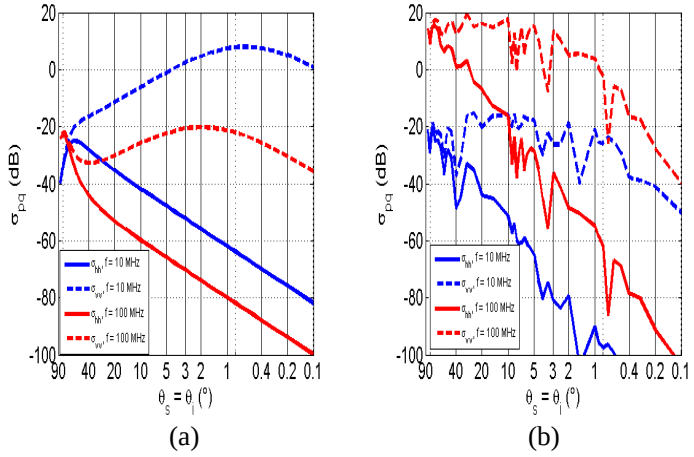

Figure 18. Observation of the RCS at grazing angles. (a) TSM. (b) SSA.

vertical and horizontal polarization, we can augment the transmitting frequency (Figure 13).

In vertical polarization, we can move the transmitter closer to the receiver (Figure 14) to increase the RCS. In horizontal polarization, the RCS is minimal when the difference between azimuthal scattered angle ϕ_s and azimuthal incident angle ϕ_i is equal to 90°.

Until 4 m/s, the increase in wind speed induces an increase in the RCS in vertical polarization (Figure 15). For windspeed greater than 4 m/s, RCS estimated by TSM decreases whereas RCS estimated by SPM, Gill's model and SSA grow. Except for SSA, RCS does not strongly differ when models are different for windspeed greater than 4 m/s. RCS estimated by Gill is near that RCS estimated by SPM when windspeed evolutes. The difference between RCS estimated by SSA and RCS estimated by the other models grows when wind speed

increases.

When the wind direction is the same that the projection of target/receiver direction in the $(\vec{x}, \vec{y})$ base, the RCS estimated by SPM or TSM in vertical polarization is maximal and this RCS is minimal when the wind direction is opposite to the projection of target/receiver direction in $(\vec{x}, \vec{y})$ base (Figure 16). The integration of RCS estimated by Gill over Doppler frequency is maximal when the wind direction is in a direction perpendicular to transmitter/target direction and it is minimal when the wind direction is the same or the opposite to the projection of transmitter/target direction in the $(\vec{x}, \vec{y})$ base (Figure 16).

The RCS estimated by TSM for a transmitting frequency of 10 MHz and the RCS estimated by SSA do not coincide with Barrick's curves (Figure 18) for grazing angles.

4.2. Ground Surface

The ground clutter RCS is simulated by SPM, TSM and SSA. Gill's model is only dedicated to sea surface. The RCS is drawn as a result of correlation length, height standard deviation, water proportion and angles for different polarizations. Vertical roughness is represented by height standard deviation. Horizontal roughness evolves inversely to correlation length.

Figure 19 shows the evolution of monostatic RCS in vertical and horizontal polarization for different height standard deviations in relation to incident angle for a correlation length of $1/k$, a relative electrical permittivity of 20 and a transmitting frequency of 25 MHz.

Figure 20 shows the evolution of monostatic RCS in vertical and horizontal polarization for different heightcorrelation lengths in

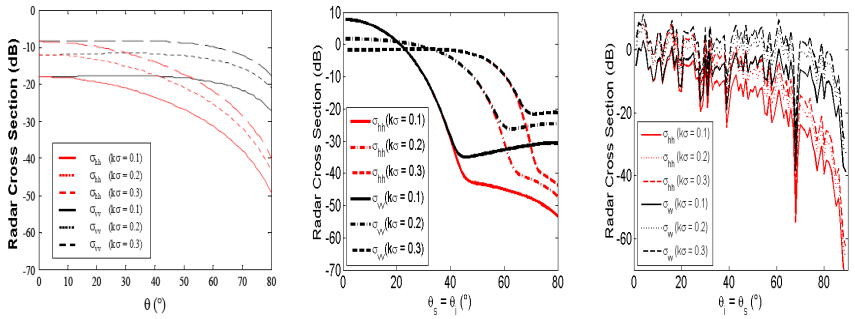

Figure 19. Evolution of the RCS in relation to the vertical roughness. (a) SPM [4]. (b) TSM. (c) SSA.

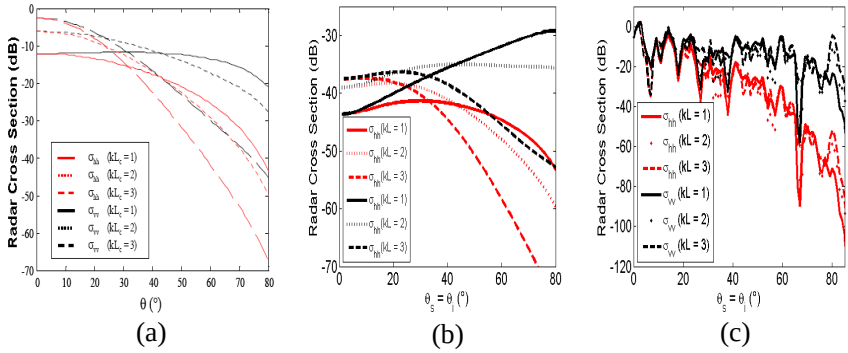

Figure 20. Evolution of the RCS in relation to the horizontal roughness. (a) SPM [4]. (b) TSM. (c) SSA.

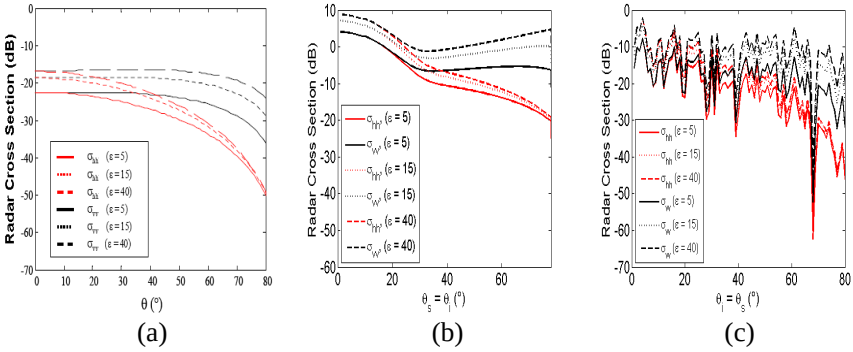

Figure 21. Evolution of the RCS in relation to the permittivity. (a) SPM [4]. (b) TSM. (c) SSA.

relation to incident angle for a standard deviation of $0.1/k$, a relative electrical permittivity of 20 and a transmitting frequency of 25 MHz.

The Figure 21 shows us the evolution in the RCS estimated by SPM, TSM and SSA related to permittivity in a vertical (vv) and horizontal (hh) polarization for a transmitting frequency of 25 MHz, a correlation length of $1/k$, a standard deviation of $0.1/k$.

According to Topp [4], a change in the water proportion modifies the electrical permittivity. To draw Figure 22(a), we used the Topp model to model permittivity for a transmitting frequency of 25 MHz, an incident angle of 75°, a scattered angle of 30°, an azimuthal incident angle of 0°, an azimuthal scattered angle of 70°, a correlation length of 5 cm and a height standard deviation of 1 cm.

Figure 23 was drawn for a transmitting frequency of 25 MHz, an

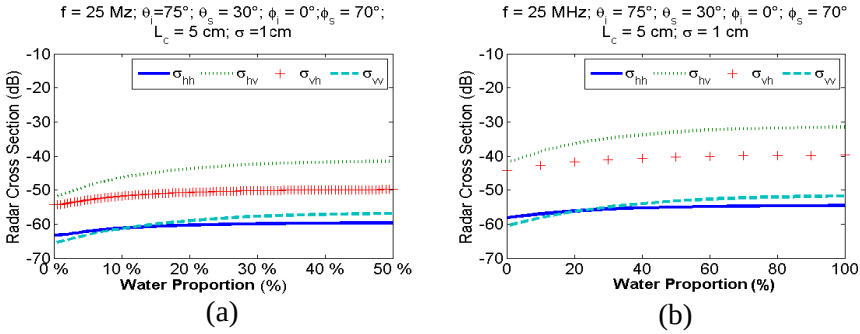

Figure 22. Evolution of the RCS in relation to the water proportion for a ground surface with $k\sigma = 0.1$ and $kL = 1$. (a) TSM. (b) SSA.

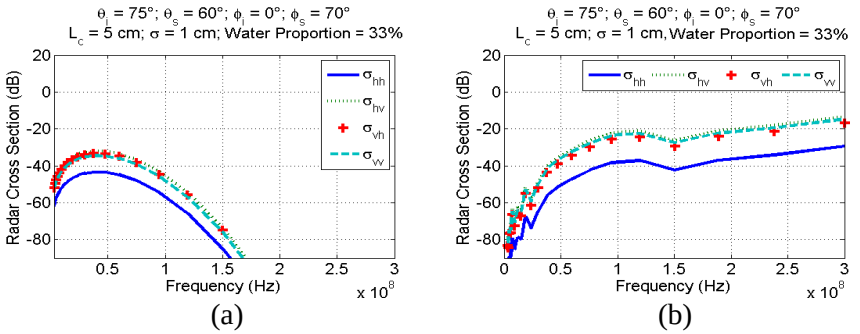

Figure 23. Evolution of the RCS in relation to the transmitting frequency. (a) TSM. (b) SSA.

incident angle of 75°, a scattered angle of 60°, an azimuthal incident angle of 0°, an azimuthal scattered angle of 70°, a correlation length of 5 cm, a height standard deviation of 1 cm and a water proportion of 33%.

Figure 24 shows us RCS estimated by TSM for a transmitting frequency of 25 MHz, an incident angle of 45°, an azimuthal incident angle of 0°, a correlation length of 5 cm, a height standard deviation of 1 cm and a water proportion of 33%.

Figure 25 shows us RCS estimated by SSA for a transmitting frequency of 25 MHz, an incident angle of 45°, an azimuthal incident angle of 0°, a correlation length of 5 cm, a height standard deviation of 1 cm and a water proportion of 33%.

As illustrated in Figure 19, when angles become grazing, the more the surface is vertically rough the high the Radar Cross Section.

In Figure 20, the Radar Cross Sections estimated by Small Slope

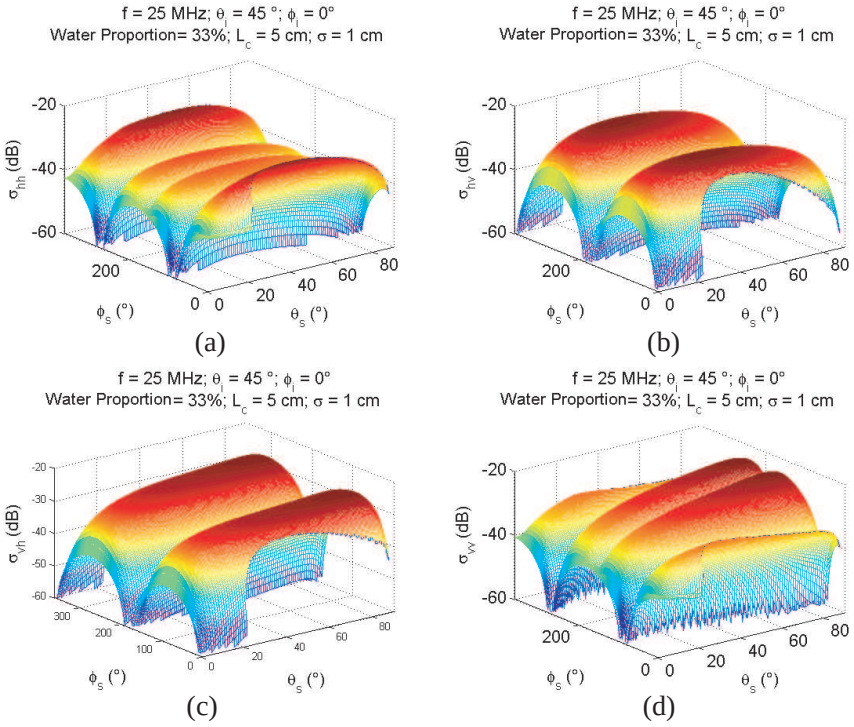

Figure 24. Evolution of the RCS in relation to the receiver position estimated by TSM. (a) σ_{hh}. (b) σ_{hv}. (c) σ_{vh}. (d) σ_{vv}.

Approximation are too wriggly to make observations in relation to horizontal roughness. As illustrated in Figure 20, when θ_i is near to normal, the more the surface is horizontally rough, the lower the Radar Cross Section. When angles become grazing, the more the surface is horizontally rough, the higher Radar Cross Section.

In Figures 19, 20 and 21, we observe that Radar Cross Section in vertical polarization is greater than Radar Cross Section in horizontal polarization and the difference between these Radar Cross Sections increases when incident angle increases. Differences between RCS estimated by TSM and others models (SPM and SSA) come from the arbitrary parameter which separate surface with large roughness from surface with small roughness.

In Figure 21, we observe that the growth in permittivity increases the RCS.

The RCS grows slowly when water proportion increases.

When frequency increases from 3 MHz to 300 MHz, the RCS

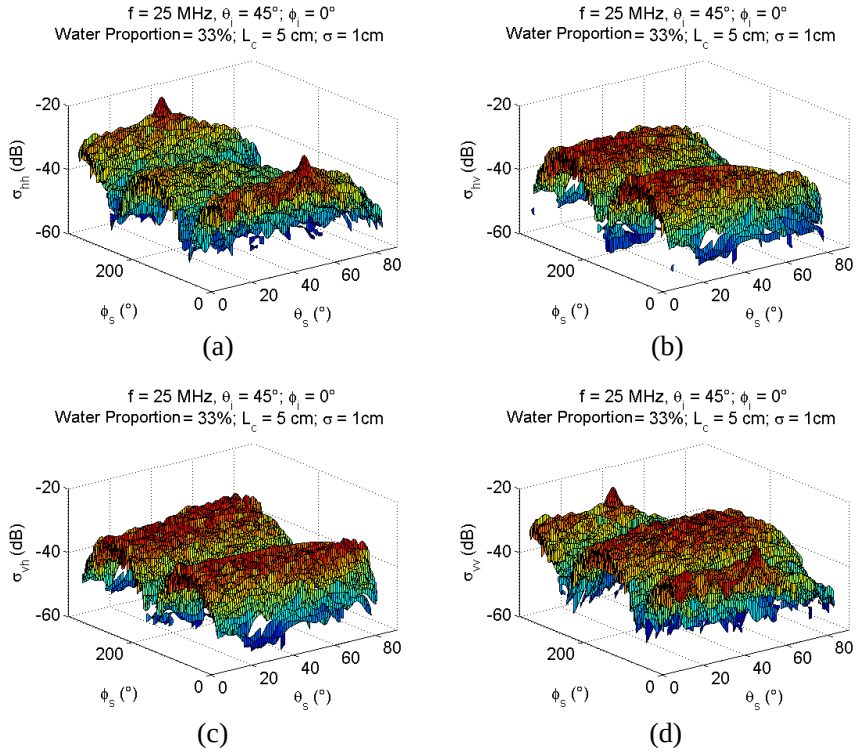

Figure 25. Evolution of the RCS in relation to the receiver position estimated by SSA. (a) σ_{hh}. (b) σ_{hv}. (c) σ_{vh}. (d) σ_{vv}.

estimated by TSM only increases to a certain point before decreasing. When the RCS is estimated using SSA, it continues to increase in this band.

Bistatic Radar Cross Section (Figures 24 and 25), in co-polarization, is maximum in specular direction and has a local maximum in backscattering direction. Bistatic Radar Cross Section in cross polarization, is minimal in specular and backscattering directions.

5. CONCLUSION

In the introduction, we examine Radar Cross Section, polarization and bistatic geometry. Then, we describe the Radar Cross Section models which we studied: Gill's model, the Kirchhoff Approximation, the Small Perturbation Model, the Two Scale Model and the Small Slope Approximation. Gill supposes that Radar Cross Section is the sum of Radar Cross Section with a single reflection, Radar Cross Section

with a double reflection to the transmitter, Radar Cross Section with a double reflection to the patch (surface) and Radar Cross Section with a double reflection to the receiver. He also makes the assumption that electrical permittivity of a surface is infinite and angles are grazing. This model is valid for a transmitting frequency between 3 MHz and 30 MHz. The model created by Gill is dedicated to a Radar Cross Section of a sea surface in a vertical (vv) polarization. The Kirchhoff Approximation is based on the hypothesis that at any point, a surface can be assimilated by its tangent. This model is valid for a surface with a mean curvature radius greater than the incidence wavelength and is applied to a surface with large roughness. For low rough surfaces, we used the Small Perturbation Model. According to the Small Perturbation Model, the total electric field can be expressed by a Fourier series with unknown amplitudes. This model is only employed for surfaces with small roughness. To take into account the double roughness of the surface, unified models such as the Two Scale Model and the Small Slope Approximation were implemented. To use the Two Scale Model, we must know the Slope probability of the surface and the Height Spectrum of the surface. The Small Slope Approximation which combines the Kirchhoff Approximation and the Small Perturbation Model. Except for Gill's model, to use Radar Cross Section models on clutter, we must know the electrical permittivity of the clutter. To model slope probability, we used the Cox and Munk model which takes wind speed and direction into account for a sea surface and a Gauss distribution for a ground surface. To model height spectrum, we used the Elfouhaily Spectrum with the Elfouhaily spread function, which takes wind speed and direction, fetch into account for a sea surface, and Gaussian spectrum which takes height standard deviation and correlation length into account for a ground surface. To model electrical permittivity, we employed the Debye model for sea surfaces which expresses electrical permittivity as a result of sea temperature, salinity and transmitting frequency. For ground surfaces, we employed the Topp model which takes into account only the water proportion.

According to these models we have studied the transmitting frequency can be decreased (less than 5 MHz) to reduce the Radar Cross Section. Sea Radar Cross Section reduces when the receiver moves away from the transmitter in vertical polarization or when the angle formed by the transmitter, the impact point and the receiver approaches 90°. RCS estimated by SPM and TSM is maximum when the wind direction is equal to the difference between scattered azimuthal angle and incident azimuthal angle. RCS estimated by SPM and TSM is minimum when the wind direction is opposite to the difference between scattered azimuthal angle and incident azimuthal

angle. Water proportion has little influence on Radar Cross Section. When angles are near normal, the rougher the ground, the lower the Radar Cross Section. When angles are grazing, the rougher the ground, the higher the Radar Cross Section. Future work would be to create an unified model (Two Scale Model or Small Slope Approximation) in relation to Doppler frequency.

REFERENCES

1. Baghdadi, N. and P. Broche, "Utilisation d'un radar océanique VHF pour la poursuite d'une balise dérivante," *Traitement du Signal*, Vol. 13, 1996.
2. Cochin, V., G. Mercier, R. Garello, V. Mariette, and P. Broche, "Anomaly detection in VHF radar measurements," *IGARSS*, Vol. 7, 4916, 2004.
3. Koudogbo, F., P. F. Combes, and H.-J. Mametsa, "Numerical and experimental validations of iem for bistatic scattering from natural and manmade rough surfaces," *Progress In Electromagnetic Research*, Vol. 46, 203–244, 2004.
4. Allain, S., "Caractérisation d'un sol nu à partir de données SAR polarimétriques Etude multi fréquentielle et multi résolution," Ph.D. Thesis, Université de Rennes, December 2003.
5. Ayari, M., "Détection électromagnétique d'éléments polluants au dessus de la surface maritime," Ph.D. Thesis, Université de Bretagne Occidentale, November 2005.
6. Barrick, D., "Grazing behaviour of scatter and propagation above any rough surface," *IEEE Transaction on Antennas and Propagation*, Vol. 46, No. 1, 73–83, January 1998.
7. Gill, E. and J. Walsh, "A perspective on two decades of fundamental and applied research in electromagnetic scattering and high frequency ground wave radar on the canadian east coast," *IGARSS*, Vol. 1, 521–523, 2002.
8. Khenchaf, A., "Bistatic scattering and depolarization by randomly rough surfaces: Application to the natural rough surfaces in X-band," *Waves in Random and Complex Media*, Vol. 11, No. 2, 61–89, October 2000.
9. Khenchaf, A., "Modélisation electromagnetique, radar bistatique et traitement de l'information," Habilitation à Diriger des Recherches, Ecole Polytechnique de l'Université de Nantes, 2000.
10. Forget, P., Y. Barbin, P. Currier, and M. Saillard, "Radar sea echo in UHF in coastal zone: Experimental observations and theory," *IGARSS*, Vol. 7, 4274–4276, 2003.

11. Vall-llossera, M., J. Miranda, A. Camps, and R. Villarino, "Sea surface emissivity modelling at L-band: An inter-comparison study," *EuroSTARRS, WISE, LOSAC Campaigns*, 2002.
12. Wan, X., X. Xiong, and H. Ke, "Ionospheric clutter suppression in HF surface wave radar OSMAR," *Antennas, Propagation and EM Theory*, 1–3, October 2006.
13. Ardhuin, F., L. Marié, N. Rascle, P. Forget, and A. Roland, "Observation and estimation of lagrangian, stokes and eulerian currents induced by wind and waves at the sea surface," *Journal of Physical Oceanography*, Vol. 39, No. 11, 2820–2838, October 2008.
14. US/EU-Baltic Int., "WERA: Remote Ocean sensing for current, wave and wind direction," *Introduction to the Principle of Operation*, 2006.
15. Saillant, S., G. Auffray, and P. Dorey, "Exploitation of elevation angle control for a 2-D HF skywave radar," *RADAR*, 662–666, 2003.
16. Bronner, E., "Amélioration des performances des radars HF à ondes de surface par étude d'antenne compacte et filtrage adaptatif appliqué à la réduction du fouillis de mer," Ph.D. Thesis, Université de Paris 9, November 2005.
17. Lipa, B. J. and D. E. Barrick, "Extraction of sea state from HF radar sea echo: Mathematical theory and modelling," *Radio Science*, Vol. 21, 81–100, January–February 1986.
18. Jangal, F., "Apport à la bipolarisation, du traitement adaptatif du signal et de la multirésolution à l'élimination du fouillis ionosphérique pour les radars hautes fréquences à ondes de surface," Ph.D. Thesis, Université Pierre et Marie Curie, November 2007.
19. Vallières, X., "Les échelles de la turbulance dans l'ionosphère des hautes latitudes et leurs signatures sur les échos des radars HF du réseau SuperDARN," Ph.D. Thesis, Université d'Orléans, December 2002.
20. Barrick, D., "Theory of HF and VHF propagation across the rough sea, 1, the effective surface impedance for a slightly rough highly conducting medium at grazing incidence," *Radio Science*, Vol. 6, No. 5, 517–526, May 1971.
21. Barrick, D., "Theory of HF and VHF propagation across the rough sea, 2, application to HF and VHF propagation above the sea," *Radio Science*, Vol. 6, 527–533, May 1971.
22. Barrick, D., "First order theory and analysis of MF/HF/VHF scatter from the sea," *IEEE Transaction on Antennas and*

Propagation, Vol. 20, No. 1, January 1972.

23. Barrick, D. and J. Snider, "The statistics of HF sea-echo doppler spectra," *IEEE Transaction on Antennas and Propagation*, Vol. 25, No. 1, January 1977.
24. Gill, E., "The scattering of high frequency electromagnetic radiation from the ocean surface: An analysis based on a bistatic ground wave radar configuration," Ph.D. Thesis, Memorial University of Newfoundland, January 1999.
25. Gill, E. and J. Walsh, "High-frequency bistatic cross section of the ocean surface," *Radio Science*, Vol. 36, No. 6, 1459–1475, November–December 2001.
26. Gill, E., W. Huang, and J. Zhang, "An alternate analysis for the second-order high frequency bistatic radar cross section of the ocean surface patch scatter and its inversion," *OCEAN*, Vol. 4, 2336–2340, 2003.
27. Gill, E., W. Huang, and J. Walsh, "On the development of a second-order bistatic radar cross section of the ocean surface: A high-frequency result for a finite scattering patch," *IEEE Journal of Oceanic Engineering*, Vol. 31, No. 4, October 2006.
28. Grosdidier, S., A. Baussard, and A. Khenchaf, "HFSW radar model: Simulation and measurement," *IEEE Transaction on Geoscience and Remote Sensing*, Vol. 48, No. 9, 3539–3549, September 2010.
29. Gill, E. and J. Walsh, "A combined sea clutter and noise model appropriate to the operation of high-frequency pulsed doppler radar in regions constrained by external noise," *Radio Science*, Vol. 43, August 2008.
30. Lewis, J. K., I. Shulman, and A. F. Blumberg, "Assimilation of doppler radar current data into numerical ocean models," *Continental Shelf Research*, 541–559, 1998.
31. Vaitilingom, L. and A. Khenchaf, "A study of radar cross section models for the ocean surface bistatic scattering applied to HFSWR radars," *OCOSS*, June 2010.
32. Lipa, B. J. and D. E. Barrick, "The second-order shallow-water hydrodynamic coupling coefficient in interpretation of HF radar sea echo," *IEEE Journal of Oceanic Engineering*, Vol. 11, No. 2, April 1986.
33. Lipa, B. J., R. D. Crissman, and D. E. Barrick, "HF radar observation of artic pack-ice breakup," *IEEE Journal of Oceanic Engineering*, Vol. 11, No. 2, 270–275, April 1986.
34. Hermansson, P., G. Forssell, and J. Fagerström, "A review

of models for scattering from rough surfaces," Technical Report, Swedish Defence Research Agency Sensor Technology, November 2003.

35. Ruffini, G., E. Cardellach, A. Rius, and J. M. Apparicio, "Remote sensing of the ocean by bistatic radar observations: A review," *Technical Report*, October 1999.
36. Daniel, S., S. Allain, and E. Pottier, "Caractérisation de la réponse sar polarimétriques d'une surface périodique par la méthode des petites perturbations," *MAJESTIC*, June 2006.
37. Sajjad, N., A. Khenchaf, and A. Coatanhay, "Electromagnetic wave scattering from sea and bare soil surfaces based on an improved two-scale model," *RADAR*, 1–6, 2009.
38. Awada, A., "Diffusion bistatique des ondes électromagnetiques par des surfaces rugueuses en utilisant le modèle SSA: Application à la surface maritime," Ph.D. Thesis, Université de Bretagne Occidentale, March 2006.
39. Cox, C. and W. Munk, "Statics of the sea surface derived from sun glitter," *Journal of Marine Research*, 198–227, February 1954.
40. Cox, C. and W. Munk, "Measurement of the roughness of the sea surface from photographs of the sun's glitter," *Journal of the Optical Society of America*, Vol. 44, No. 11, 838–850, November 1954.
41. Cox, C. and W. Munk, "Slopes of the sea surface deduced from photographs of sun glitter," *Scripps Institution of Oceanography*, Vol. 6, 401–487, September 1956.
42. Melsheimer, C. and L. K. Keong, "Sun glitter in spot images and the visibility of oceanic phenomena," *22nd Asian Conference on Remote Sensing*, 870–875, November 2001.
43. Elfouhaily, T., B. Chapron, K. Katsaros, and D. Vandemark, "A unified directional spectrum for long and short wind-driven waves," *Journal of Geophysical Research*, Vol. 102, No. 15, 781–796, July 1997.
44. Klein, L. and C. Swift, "An improved model for the dielectric constant of sea water at microwave frequencies," *IEEE Transactions on Antennas and Propagation*, Vol. 25, No. 1, January 1977.